CONSTITUTIVE MODELING FOR ISOTROPIC MATERIALS*

Ulric S. Lindholm and Kwai S. Chan
Southwest Research Institute

INTRODUCTION

The objective of the present program is to evaluate and further develop existing constitutive models for use in finite-element structural analysis of turbine engine hot section components. The class of constitutive equation studied is considered "unified" in that all inelastic deformation including plasticity, creep, and stress relaxation are treated in a single term rather than a classical separation of plasticity (time independent) and creep (time dependent) behavior. The unified theories employed also do not utilize the classical yield surface or plastic potential concept. The models are constructed from an appropriate flow law, a scalar kinetic relation between strain rate, temperature and stress, and evolutionary equations for internal variables describing strain or work hardening, both isotropic and directional (kinematic). This and other recent studies have shown that the unified approach is particularly suited for determining the cyclic behavior of superalloy type blade and vane materials and is entirely compatible with three-dimensional inelastic finite-element formulations.

In the first two years of the program, the unified constitutive models of Walker (ref. 1) and of Bodner and Partom (ref. 2) were demonstrated to yield good correlation for a nickel-base alloy (PWA designation B1900+Hf) for temperatures, strain rates, and strain range characteristic of cooled turbine vanes in advanced gas turbine engines. Experimental correlations were made with testing under uniaxial and biaxial tensile, creep, relaxation, cyclic, and TMF loading histories. Both models were incorporated into the MARC finite-element computer code. The code was then utilized to predict the high-temperature cyclic response of a notched-round tensile bar.

In this, the third year of the program, we have examined the behavior of a second nickel-base alloy, MAR-M247, and compared it with the Bodner-Partom model, further examined procedures for determining the material-specific constants in the models, and exercised the MARC code for a turbine blade under simulated flight spectrum loading. The third year results will be summarized in the following sections. Collaborators on this program have been staff of Pratt and Whitney Aircraft and Drs. Walker and Bodner.

TEST PROCEDURES AND APPLICATION TO MAR-M247 AND B1900+Hf

The details of both Bodner-Partom and Walker models and experimental facilities and test procedures are fully described in the Second Annual Status Report under this project (NASA CR-174980). Therefore, we will summarize only current results herein.

---

*Work done under NASA Contract NAS3-23925.

Uniaxial monotonic hardening. A major concern with the unified or any other comprehensive constitutive model is the determination of the material constants and the number of test conditions required in the process. Our previous work, to our surprise, had indicated that all constants could be derived from monotonic tensile tests alone conducted over the appropriate temperature and strain-rate ranges. It is usually assumed that cyclic data are required to separate the directional or kinematic hardening terms. However, it should be realized that hardening under any loading history results from both isotropic and directional components which may be separated if a model is available.

The monotonic tensile curves for MAR-M247 at several temperatures are given in Figure 1a with the Bodner-Partom model correlation below in Figure 1b. The hardening constants for the model correlation are determined from the construction given in Figure 2. Here the work-hardening rate, $\gamma = d\sigma/dW_p = d\sigma/\sigma d\varepsilon^p$, is plotted as a function of applied stress by differentiating the stress-plastic strain curve. A common assumption, used in the Bodner-Partom model, is that both isotropic and directional hardening progresses from an initial or current state to a satauration value ($d\sigma/dW_p = 0$) with large strain at a hardening rate determined by the parameter m. Such an evolutionary equation for hardening is

$$\dot{h} = m(h_s - h)\dot{W}_p$$

where h is the current state, h_s is the saturation value, and m is the rate parameter. One can show from the construction in Figure 2 that m_1 is the rate of isotropic hardening and that m_2 is the rate of directional hardening. Further, the saturation values, h_s, for both can be obtained from the stress intercept at $\gamma = 0$. Directional hardening saturates first and dominates at small strain, while the isotropic hardening dominates at large strains.

Figures 2b and 2c demonstrate similar hardening behavior for two other high-temperature alloys, B1900+hf and Hastelloy X.

Cyclic response prediction. The cyclic stress-strain curve predicted from the Bodner-Partom model and the monotonic tensile test data are given in Figure 3b along with the experimental curves in Figure 3a. Extensive similar correlations for B1900+Hf are given in NASA CR-174980 for cycles with varying strain range, R-ratio, hold-times, and temperature (TMF).

Biaxial response. Extensive biaxial tests have been conducted also on thin tubes under combined tension-compression and reversed torsion. Two examples will be cited. In Figure 4 we illustrate an experiment-model comparison for MAR-M247 tested at 982°C. Out-of-phase, strain-controlled loading is employed with the von Mises effective strain held constant during cycling but with periodic strain hold-times to observe the direction and magnitude of the stress relaxation. The Bodner-Partom model predicts the essential features except for the transient direction of the stress vector during relaxation. The model prescribes this direction to be radial toward the stress origin. The experiment shows that only asymptotically at long time is the relaxation vector in the direction of the origin. Also (not shown), the instantaneous direction of the strain-rate vector during the active cyclic portion of the loading is not radial (Bodner-Partom model prediction) but shows a small phase lag from the radial direction. An alternate model, such as that of Walker (ref. 1) which employs a "back-stress" type representation for directional hardening, does a more accurate prediction of these vectorial effects.

Figure 5 shows that for alloy B1900+Hf the cyclic hardening under out-of-phase and in-phase cycling was equal. The same result was found for MAR-M247 at all temperatures. This contrasts with previous results on Hastelloy X where the cyclic hardening under out-of-phase cycling was considerably greater than under in-phase (proportional) cycling.

Variable strain-rate tests. A series of tests was performed on MAR-M247 at several temperatures which included step-wise changes in strain rate. The results are illustrated in Figure 6. One purpose of these tests was to determine if both the hardening and rate-dependent constants in the Bodner-Partom model could be determined from a single test (specimen) at a given temperature. The result was partially successful in that the constants derived were used in the model correlations shown. However, the constants derived showed some differences from a set derived from multiple specimens each tested at a different strain rate. The latter procedure would be preferred, although a good first approximation can be obtained from the step-loaded single specimen.

HOT SECTION COMPONENT ANALYSIS

The component chosen for demonstration of the B1900+Hf unified model is the airfoil portion of a typical cooled turbine blade. The foil was analyzed using the MARC finite element program (ref. 3). The code was used at PWA with the Walker model and subsequently at NASA Lewis (ref. 4) with both the Walker and Bodner-Partom models for comparison. Figure 7a shows the finite element mesh used in the analysis. The bulk of the airfoil was modeled with 8-node solid elements with regions on the leading edge modeled with higher order 20-node solid elements. Figure 7b shows the temperature distribution during the cruise portion of the flight spectrum.

The loading and boundary conditions were chosen to simulate a typical commercial engine flight. The flight simulation is shown schematically in Figure 8 and includes periods of taxi, takeoff, climb, cruise, descent, taxi, and shutdown. The spectrum includes periods of transient loading (RPM) and temperature excursions as well as long steady-state or hold periods. The maximum temperature excursion is about 1000°C. Thus, the range of conditions exercises the constitutive model over a wide range of the state parameters.

PWA exercised the foil through three full flight spectra using the Walker model. Figure 9 shows the accumulation of inelastic strain at location A (Figure 7b) during all three flights. It is seen that the bulk of the inelastic strain is accumulated during takeoff of the first flight. At the end of climb some reversed inelastic strain is accumulated up to shutdown at this element. After the third flight the amount of inelastic strain accumulation appears to be stabilizing.

Using the PWA-developed code with identical mesh size and flight spectra, Kaufman et al (ref. 4) ran further simulations comparing a classical creep-plasticity model with both the Walker and Bodner-Partom unified models. The effective stress vs strain response at the airfoil critical location is compared in Figure 10 for all three constitutive models. The unified models yield very similar results but substantially different from the classical creep-plasticity model. Unfortunately, no experimental results are available or easily obtainable for this complex problem. It is noteworthy that a comparison of the CPU time requirements for these analyses on a Cray computer indicates that there is essentially no difference between the classical and unified approaches. For the problem cited, the CPU time was about 4000 sec with each model.

CONCLUSIONS AND FUTURE WORK

The results to date have further demonstrated the ability of the unified constitutive equations to model complex nonlinear, time- and temperature-dependent inelastic deformation under complex loading conditions. A methodology for evaluating the constitutive constants in the models from simple test conditions is evolving. The demonstration that these improved models can be used in a general-purpose, finite-element structural analysis code without penalty in computing time over existing methods is significant.

In the final year of the program we will examine further the effects of thermal history on the constitutive behavior of these nickel-base alloys with possible modifications to the models to include effects of strain aging, microstructural changes, and thermal history. Some experiments are also planned to assess the effect of a thermal-barrier coating on the response of thin-walled, biaxial tubular specimens.

REFERENCES

1. Walker, K. P.: NASA Contract Report NASA CR-165533, 1981.

2. Bodner, S. R. and Partom, Y: ASME J. of Appl. Mechs., vol. 42, 1975.

3. MARC General Purpose Finite Element Program, MARC Corporation, Palo Alto, California.

4. Kaufman, A., Saltsman, J. F., Halford, G. R., and Tong, M.: 3rd Symposium on Nonlinear Constitutive Relations for High Temperature Applications, Akron, Ohio, 1986.
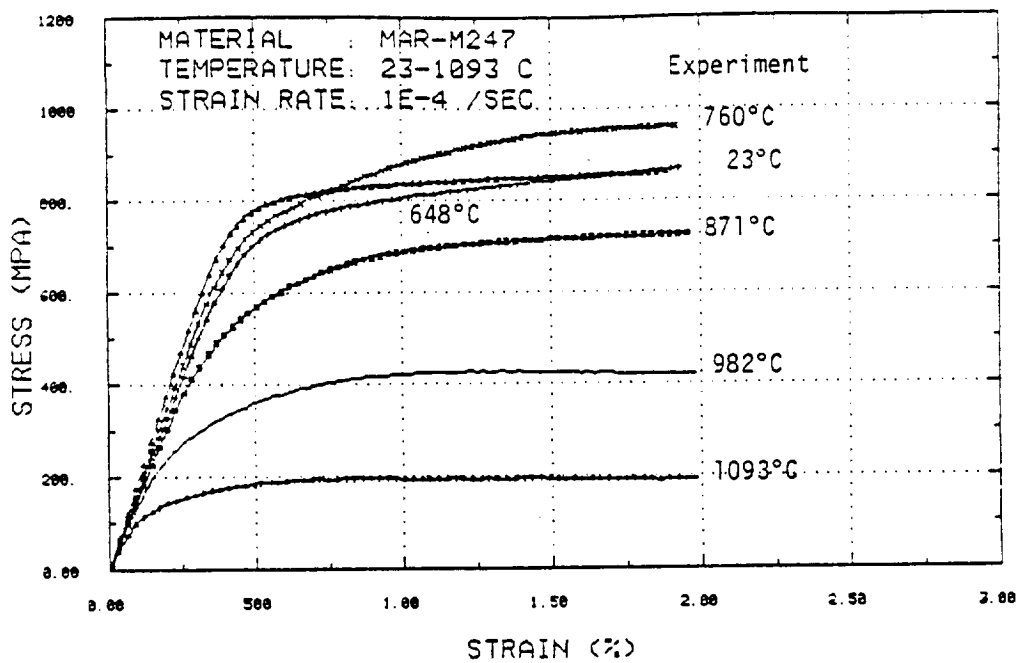
(a)
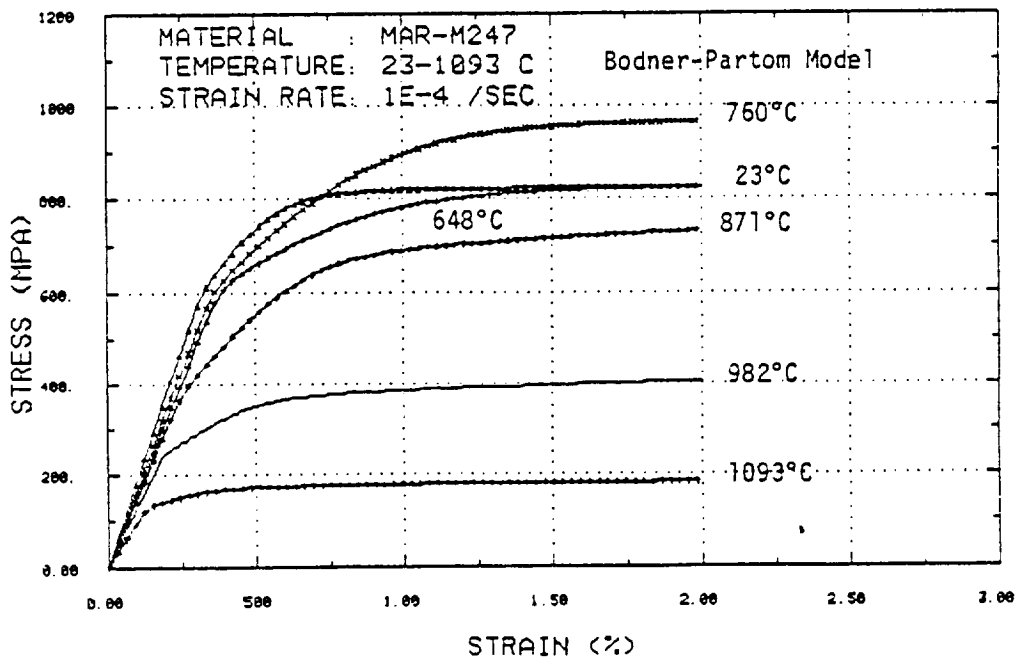
(b)

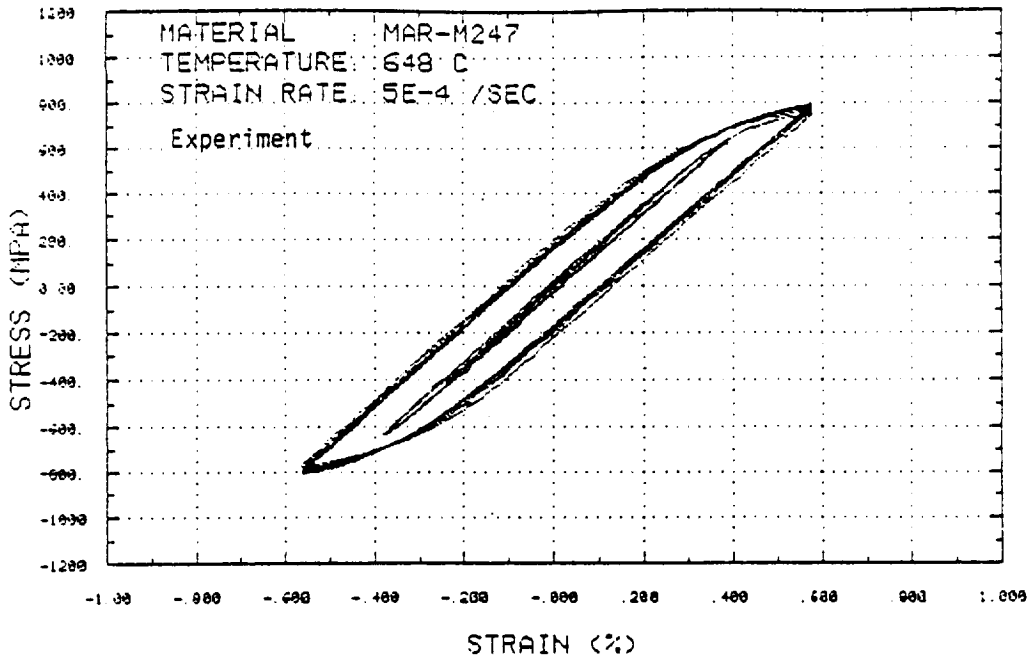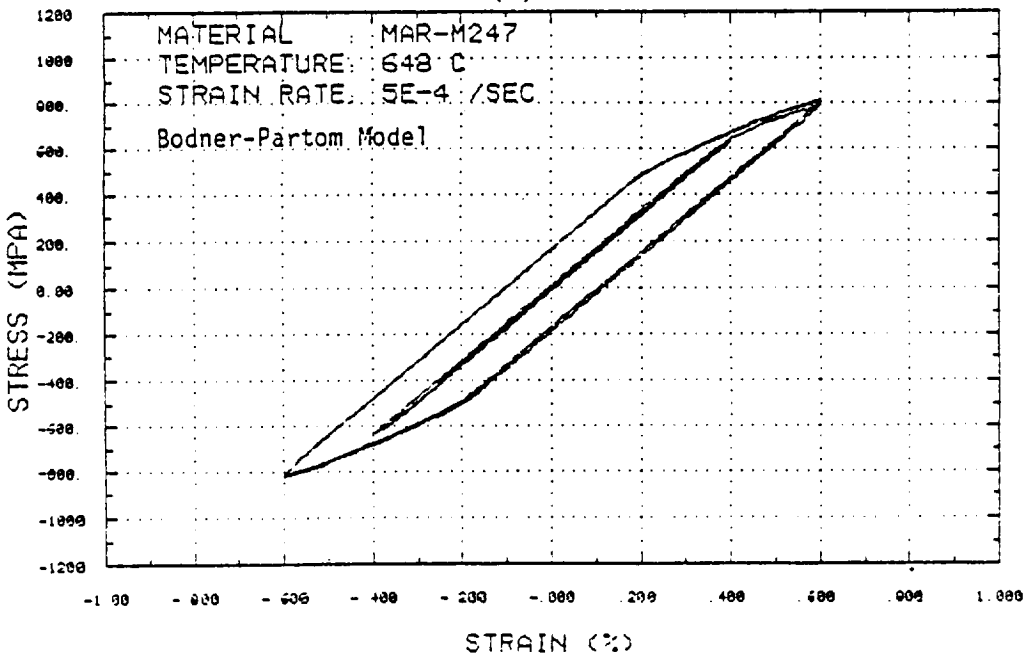Figure 1. Correlation of Bodner-Partom model (b) with experimental tensile curves (a) for MAR-M247 at six temperatures.
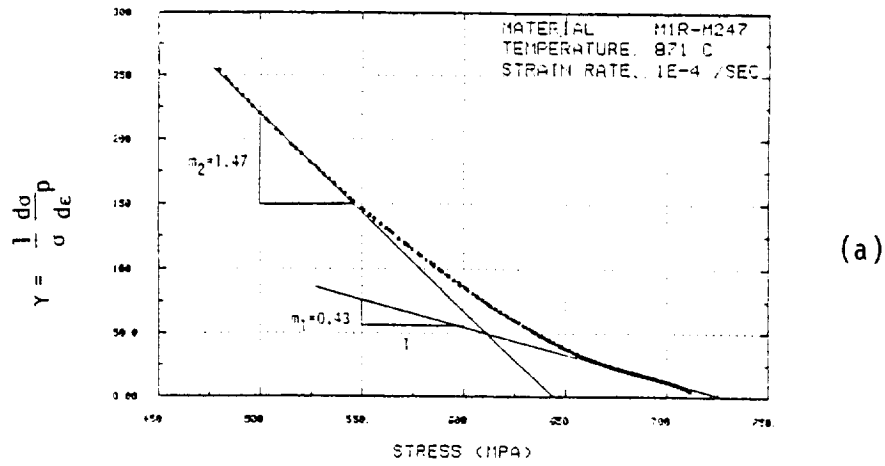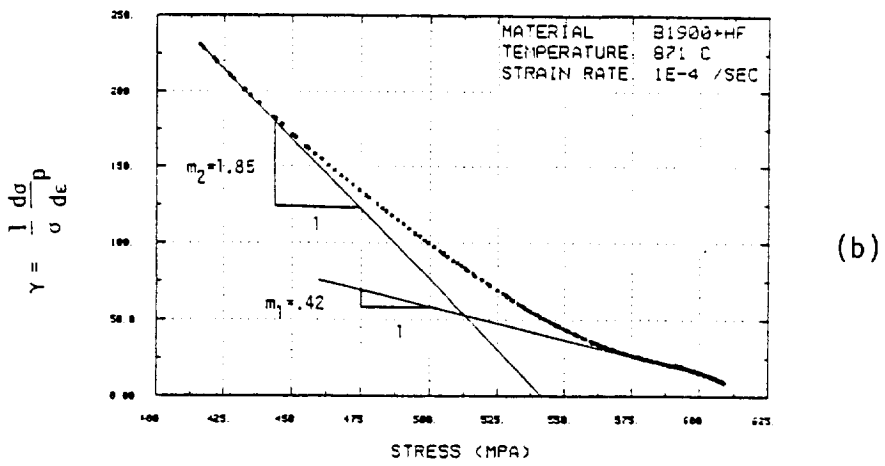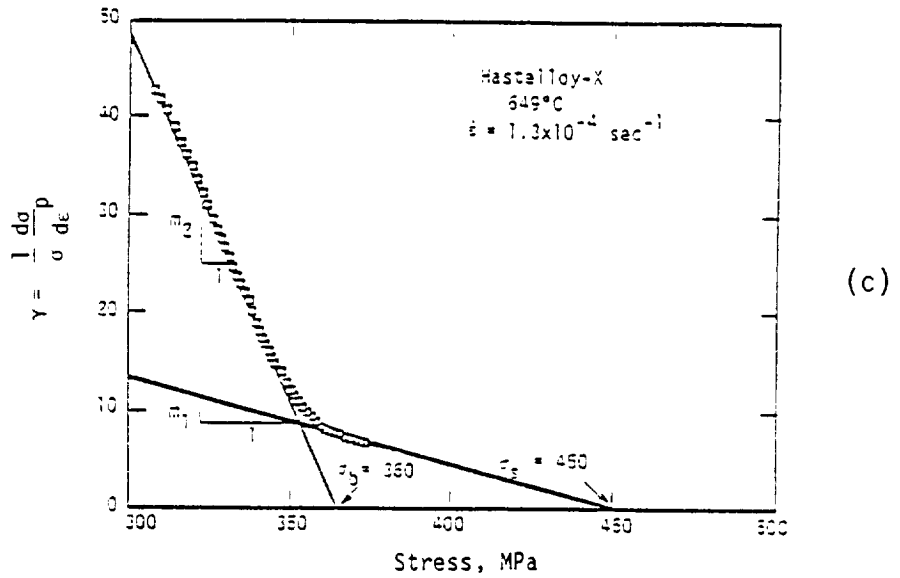
Figure 2. The work hardening curves for (a) MAR-M247, (b) B1900+Hf, and (c) Hastelloy X showing separation of isotropic and directional hardening parameters.

Figure 3. Comparison of model prediction (b) and experimental cyclic data (a) at 648°C for MAR-M247.
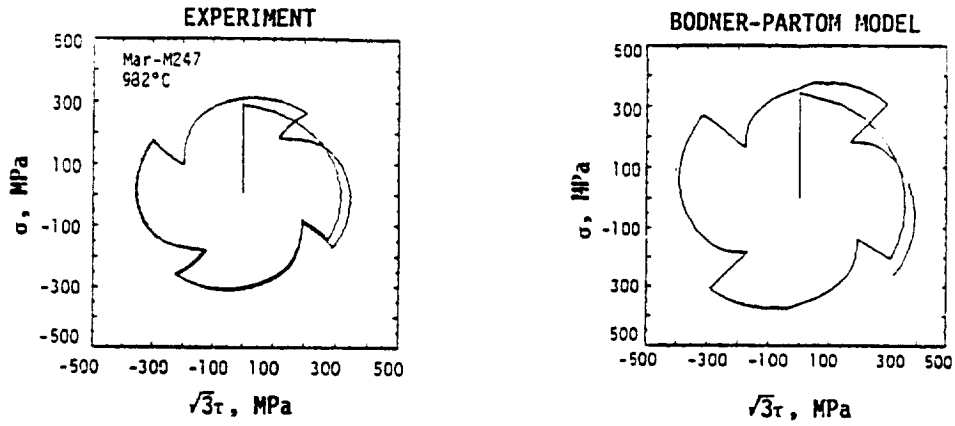
Figure 4. Comparison of model calculation and experiment for MAR-M247 under 90° out-of-phase cycling with hold time at 982°C.
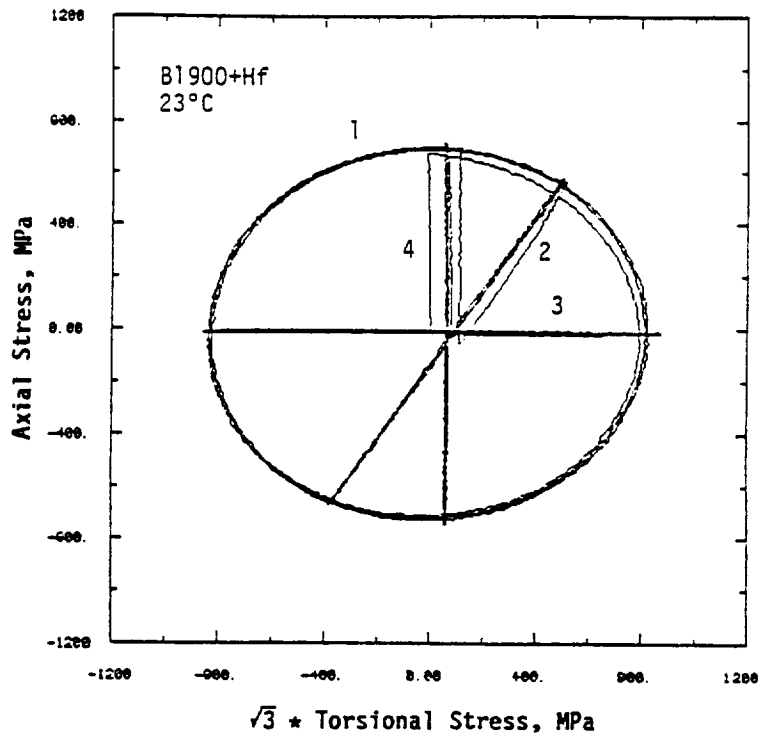
Figure 5. The stress response of B1900+Hf tested under (1) 90° out-of-phase axial/torsion, (2) in-phase axial/torsion, (3) torsion, and (4) axial. Effective strain and strain rate are ±0.4% and 4×10^{-1} sec^{-1}.
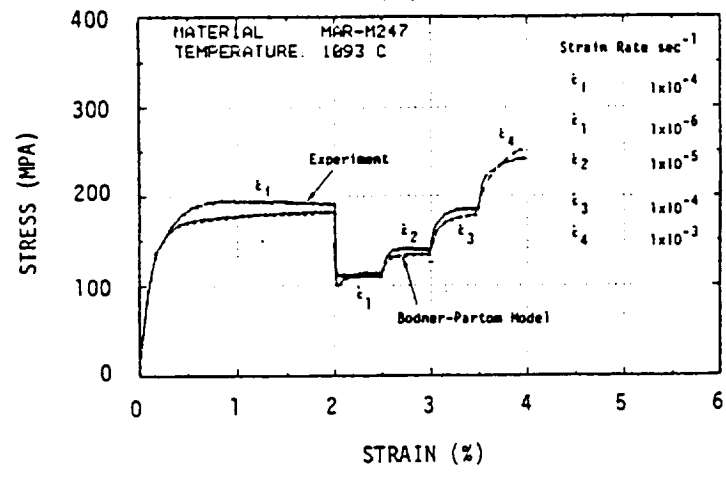
250
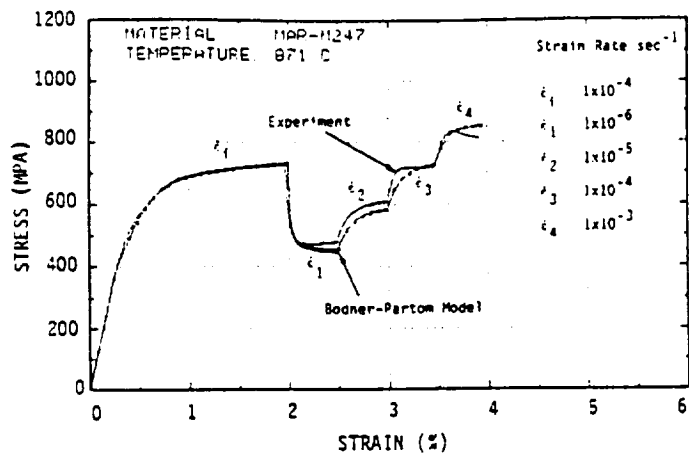
(a)
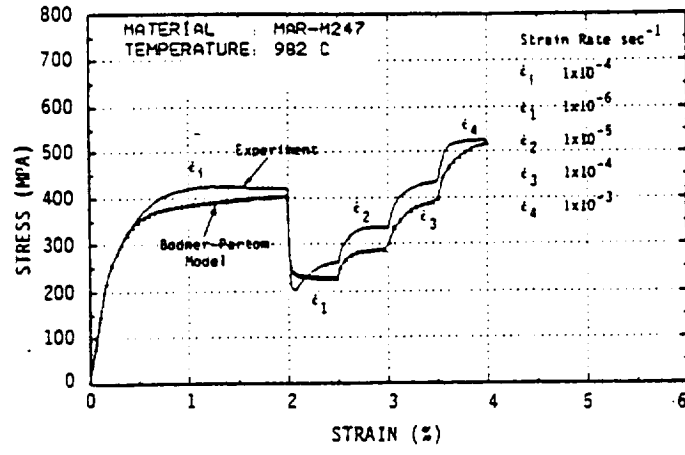
(b)

(c)

Figure 6. Comparison of model calculation and experiment for tensile test with step strain-rate changes; MAR-M247 at (a) 871°C, (b) 982°C, and (c) 1093°C.

(a)   (b)
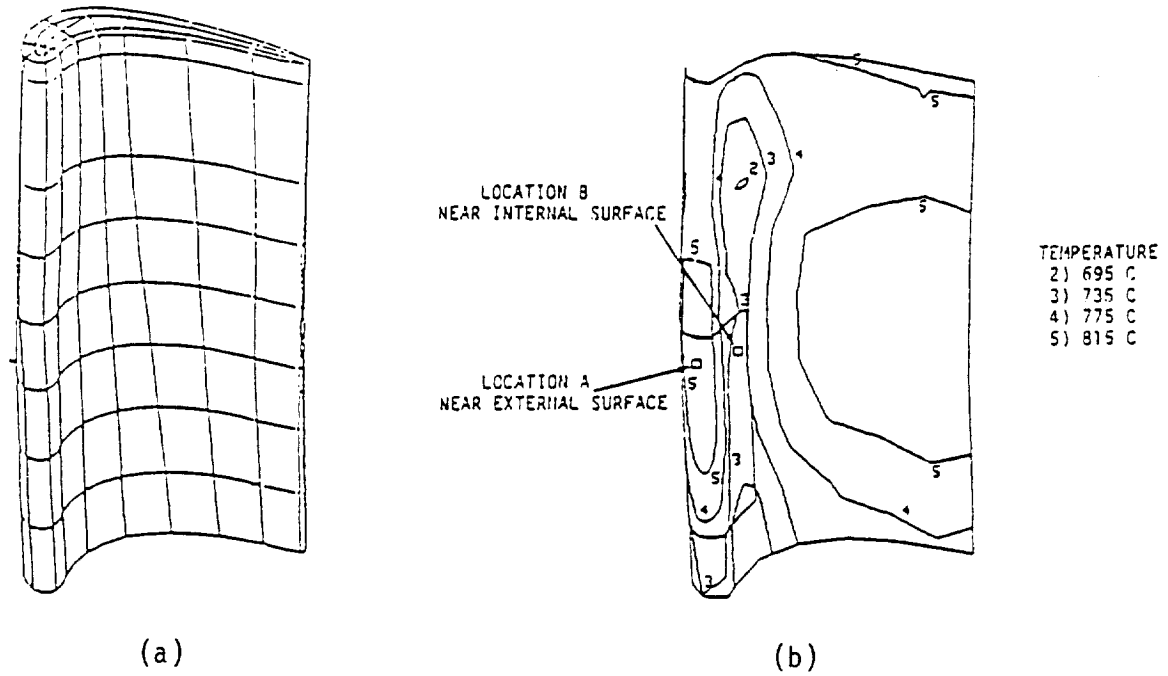
Figure 7.   Finite element mesh used in calculation (a) and steady-state
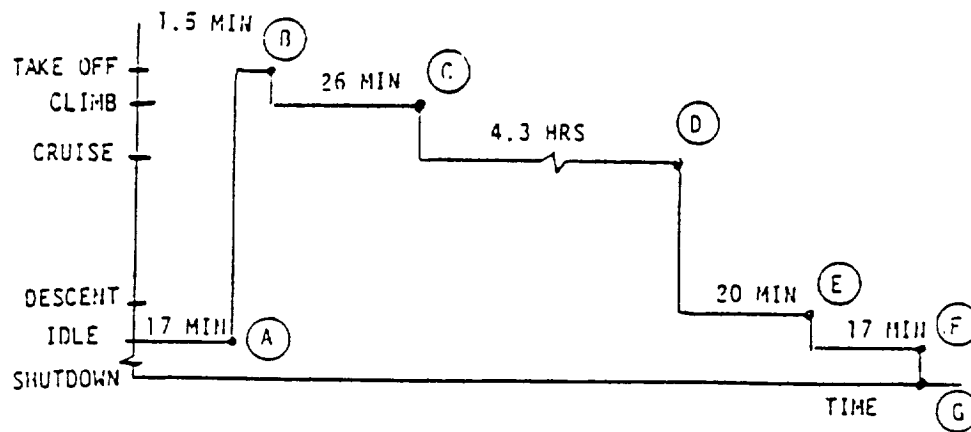   temperature profile during cruise (b).

Figure 8.   Simulated flight used in demonstration calculations
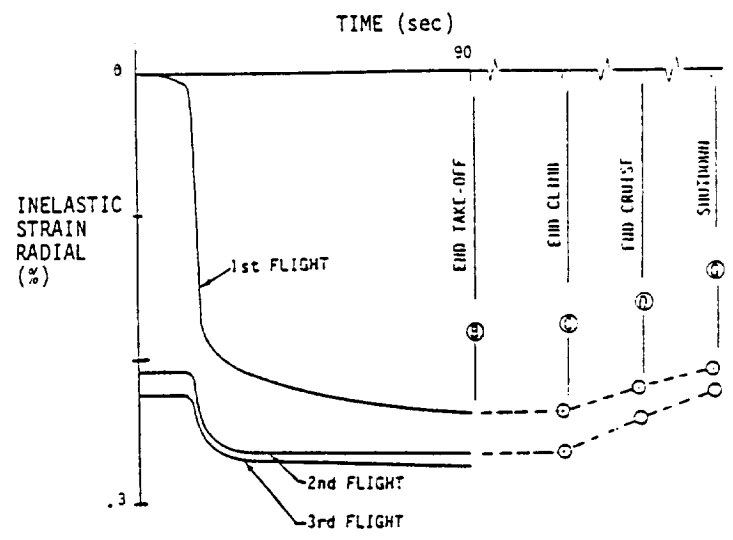
Figure 9. Accumulation of inelastic strain at location A (Figure 7) during all three flights.
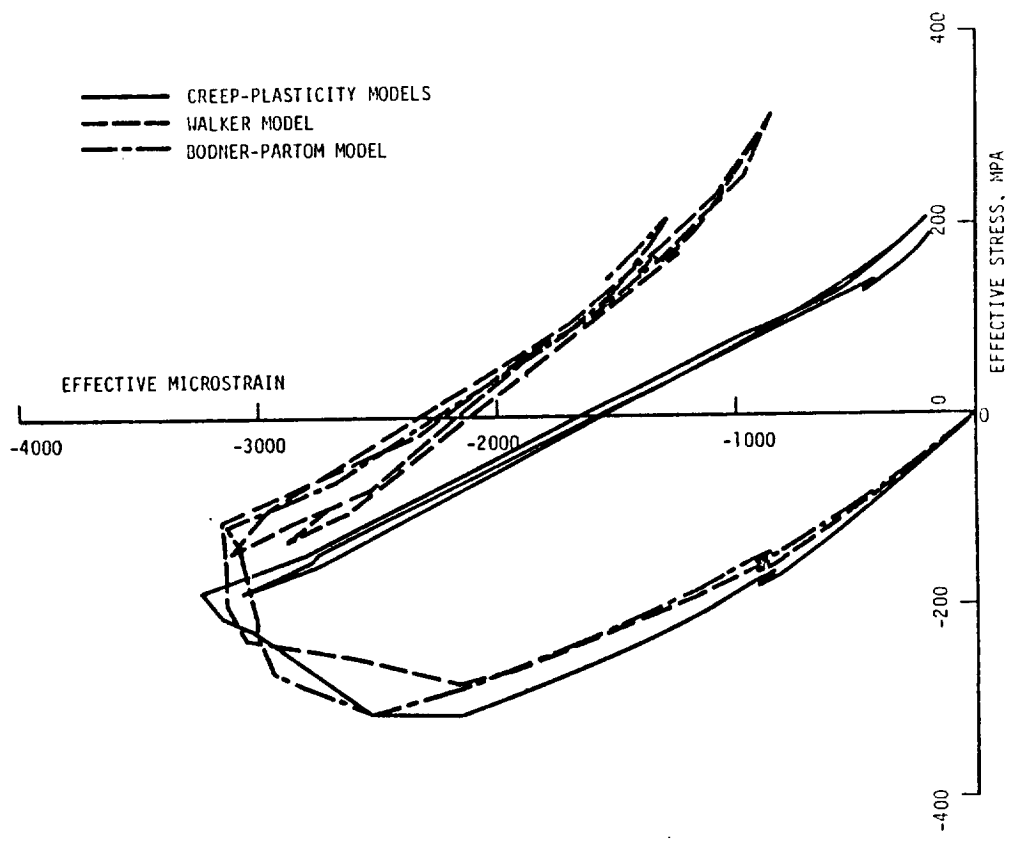

Figure 10. Airfoil calculations using the MARC finite-element analysis code from Kaufman et al (ref. 4).

253